Heterosubtypic influenza protection elicited by double-layered polypeptide nanoparticles in mice

Lei Deng[a], Timothy Z. Chang[b], Ye Wang[a], Song Li[b], Shelly Wang[c], Shingo Matsuyama[a], Guoying Yu[d], Richard W. Compans[c], Jian-Dong Li[a], Mark R. Prausnitz[b], Julie A. Champion[b], and Bao-Zhong Wang[a,1]

[a]Center for Inflammation, Immunity & Infection, Georgia State University Institute for Biomedical Sciences, Atlanta, GA 30303; [b]School of Chemical & Biomolecular Engineering, Georgia Institute of Technology, Atlanta, GA 30332; [c]Emory Vaccine Center, Department of Microbiology and Immunology, Emory University School of Medicine, Atlanta, GA 30307; and [d]State Key Laboratory of Fibrosis Biology, College of Life Science, Henan Normal University, Xinxiang, 453002 Henan, China

Edited by Peter Palese, Icahn School of Medicine at Mount Sinai, New York, NY, and approved July 9, 2018 (received for review April 5, 2018)

Influenza is a persistent threat to public health. Here we report that double-layered peptide nanoparticles induced robust specific immunity and protected mice against heterosubtypic influenza A virus challenges. We fabricated the nanoparticles by desolvating a composite peptide of tandem copies of nucleoprotein epitopes into nanoparticles as cores and cross-linking another composite peptide of four tandem copies of influenza matrix protein 2 ectodomain epitopes to the core surfaces as a coating. Delivering the nanoparticles via dissolvable microneedle patch-based skin vaccination further enhanced the induced immunity. These peptide-only, layered nanoparticles demonstrated a strong antigen depot effect and migrated into spleens and draining (inguinal) lymph nodes for an extended period compared with soluble antigens. This increased antigen-presentation time correlated with the stronger immune responses in the nanoparticle-immunized group. The protection conferred by nanoparticle immunization was transferable by passive immune serum transfusion and depended partially on a functional IgG receptor FcγRIV. Using a conditional cell depletion, we found that CD8$^+$ T cells were involved in the protection. The immunological potency and stability of the layered peptide nanoparticles indicate applications for other peptide-based vaccines and peptide drug delivery.

influenza A virus | universal influenza vaccine | epitope | nanoparticle | microneedle

Suboptimal protection (from 10 to 60%) by seasonal influenza vaccines correlates with severe epidemic outbreaks (1). Scientists have recognized the impossibility of always designing an effective influenza vaccine based on recent circulating strains. A universal influenza vaccine that can induce broad and effective protection against a wide range of influenza viruses is needed to eliminate the threats of influenza epidemics and pandemics (2, 3).

Nucleoprotein (NP), an internal influenza protein, is a vaccine target of interest because it induces cross-protection against diverse influenza A virus challenges (4). Cross-reactive CD8$^+$ cytotoxic T cell responses to conserved influenza epitopes correlate to less severe and shorter illnesses in humans (5). While natural infection can induce NP-specific CD8$^+$ cytotoxic T cell responses that are resilient to antigenic drift, inactivated influenza vaccines inefficiently stimulate these responses (6, 7). However, universal influenza vaccine MVA-NP-M1 coadministered with seasonal influenza vaccines in aged adults increased strain-specific antibody responses and boosted cross-reactive memory T cell responses (8). In this study, we intended to expand the immunity by coadministration of inactivated influenza vaccines with our designed layered peptide-only nanoparticles.

The amino acid sequence of the ectodomain of influenza A M2 protein (M2e) is conserved among most human seasonal influenza A viruses and is a promising target for universal influenza vaccines (9–12). Natural human influenza A infection induces weak, short-lived M2e-specific immunity (13). Increasing the copy number of M2e in an immunogen significantly enhances the specific immune responses and reduces the number of vaccinations required for complete protection against a lethal influenza A challenge (14).

Nanotechnology provides a promising approach for the development of new generations of influenza vaccines. Physiologically activated disassembling nanoparticles mimic the biophysical and biochemical cues of virions and initiate "danger" signals that enhance the activation of innate immunity and elicit potent cellular and humoral immune responses with minimal cytotoxicity (15). Protein nanoparticles stimulate dendritic cell maturation and elicit the production of the inflammatory cytokine IL-1β in vitro (16, 17). Incorporating immunostimulatory materials enables nanoparticles to activate antigen presenting cell (APC) maturation and to avoid immune tolerance (18–20). Nanoparticles have the versatility to incorporate any peptide- or protein-based adjuvant or antigen, but the risk of loss of antigenicity and immunogenicity during particle synthesis has hampered nanoparticle vaccine development (17, 21). Here, we explored methods to incorporate the composite peptides into nanoparticles without the loss of antigenicity and immunogenicity.

Peptide-based vaccines containing minimal epitopes can protect against pathogens and cancers. An increasing number of peptide-based influenza vaccines are in clinical trials (22). However, peptides are often weakly immunogenic and require particulate carriers for delivery or the use of adjuvants for the

Significance

Mismatched seasonal influenza vaccines are low efficacy and provide limited protection against circulating strains. A universal influenza vaccine that can induce broadly cross-protective immunity is urgently needed. Here, we have developed a layered peptide-only nanoparticle vaccine delivered by dissolvable microneedle patches. Immunizations with the vaccine candidates elicited robust long-lasting protective immune responses in mice. We found that the unique in vivo biodistribution feature of the nanoparticles correlated with the long-term immunity. This vaccine approach can be applied to develop peptide-based vaccines for different pathogens.

Author contributions: B.-Z.W. designed research; L.D., T.Z.C., Y.W., S.L., S.W., S.M., R.W.C., M.R.P., J.A.C., and B.-Z.W. performed research; S.L., S.W., S.M., G.Y., R.W.C., J.-D.L., M.R.P., and J.A.C. contributed new reagents/analytic tools; L.D., T.Z.C., Y.W., G.Y., R.W.C., J.-D.L., M.R.P., J.A.C., and B.-Z.W. analyzed data; and L.D. and B.-Z.W. wrote the paper.

Conflict of interest statement: L.D. and B.-Z.W. are inventors on patents and patent applications related to this study. M.R.P. is an inventor of patents licensed to companies developing microneedle-based products, is a paid advisor to companies developing microneedle-based products, and is a founder/shareholder of companies developing microneedle-based products (Micron Biomedical).

This article is a PNAS Direct Submission.

[1]To whom correspondence should be addressed. Email: bwang23@gsu.edu.

This article contains supporting information online at www.pnas.org/lookup/suppl/doi:10.1073/pnas.1805713115/-/DCSupplemental.

Published online July 31, 2018.

induction of strong immune responses. Our previously fabricated protein nanoparticles boosted the immunogenicity of the comprising proteins. Here, we explored if the layered nanoparticle format can boost the immunogenicity of the composite peptides without the use of adjuvants.

Skin vaccination with dissolvable microneedle (MN) patches offers many logistical and immunological advantages over traditional intramuscular (IM) injection (23–25). An MN patch contains an array of solid, water-soluble, submillimeter MNs that encapsulate antigen and can be easily and painlessly self-administered (26). Skin vaccination is immunologically advantageous because of the large numbers of APCs present in the skin tissues, such as Langerhans cells and other dendritic cells (10, 23, 25). The present study examined the efficacy of MN skin vaccination with the layered peptide nanoparticles.

We have previously demonstrated that layered protein nanoparticles comprised M2e protein cores with headless hemagglutinin (HA) proteins cross-linked to the surfaces induced immune protection predominantly through antibody responses in mice (27). While humoral immunity is useful and can protect mice from heterologous influenza challenges, T cell immunity provides appreciated cross-protection and correlates with early recovery from infection (28, 29). The present work studied the level of protection, the mode of the protection induced, if robust T cell immunity could be elicited by the layered peptide nanoparticles comprised NP peptide cores and M2e peptide coatings, and if T cell epitopes in the cores can induce a helper T cell response synergizing the antibody response to B cell antigens in the coatings.

In this study, we have designed and tested peptide-only layered nanoparticles and MN patch vaccines, and explored the protection mechanisms.

Results

Characterization of Fabricated Peptide Nanoparticles. We constructed a composite peptide including three tandem copies of both NP epitopes NP_{147} (TYQRTRALV) and NP_{55} (RLIQNSLTIERMVLS) (30–32) (Fig. 1*A*, *Upper*). Sequences of NP_{147} and NP_{55} are highly conserved among 18,540 human influenza A NP sequences deposited in the Influenza Research Database (IRD website: https://www.fludb.org/brc/home.spg?decorator=influenza) (*SI Appendix*, Fig. S1). We also constructed and produced a peptide with M2e consensus sequences from human, swine, and avian influenza strains (designated 4M2e) (Fig. 1*A*, *Lower*). We confirmed the expression of the NP peptide and 4M2e by Western blots using an anti–His-tag monoclonal antibody (Fig. 1*B*).

We desolvated the NP peptide or NP protein from the H3N2 strain (A/Aichi/2/1968) into nanoparticles as cores (NP-peptide nanoparticles and NP-protein nanoparticles) and cross-linked 4M2e onto the cores as a coating layer to generate NP-peptide/4M2e or NP-protein/4M2e double-layered nanoparticles (diagrammed in Fig. 1*C*). A peptide (pep-23) (*SI Appendix*, Table S1) and the NP peptide were desolvated into smaller nanoparticles (142 ± 48 nm and 157 ± 61 nm, respectively) than the NP protein or IgG (*SI Appendix*, Fig. S2*A*). The nanoparticle yield from peptides (pep-23, 22.3%; NP peptide, 60.2%) was lower than from proteins (the NP protein or IgG, over 85%) (*SI Appendix*, Fig. S2*B*). The average diameters of NP-peptide/4M2e and NP-protein/4M2e–layered nanoparticles expanded with the amount of 3,3′-dithiobis(sulfosuccinimidyl propionate) (DTSSP) (from 0 to 100 mM concentration) used following ethanol desolvation and coating (*SI Appendix*, Fig. S2*C*).

Dynamic light scattering analysis revealed an average hydrodynamic diameter of 163 ± 69 nm for NP-peptide nanoparticles, 183 ± 58 nm for NP-peptide/4M2e–layered nanoparticles, 211 ± 76 nm for NP-protein nanoparticles, and 228 ± 82 nm for NP-protein/4M2e–layered nanoparticles (Fig. 1*D*), demonstrating a slight increase in nanoparticle size due to the cross-linked coatings. Scanning electronic micrography revealed that the nanoparticles were relatively spherical with irregular surfaces (Fig. 1*E*). Soluble unbound or self–cross-linked 4M2e could not be pelleted in a high-speed centrifugation (33). In a pull-down assay, a trace amount (around 3%) of uncoated NP-peptide (core only) nanoparticles existed in the NP-peptide/4M2e–layered nanoparticle sample (*SI Appendix*, Fig. S2*D*).

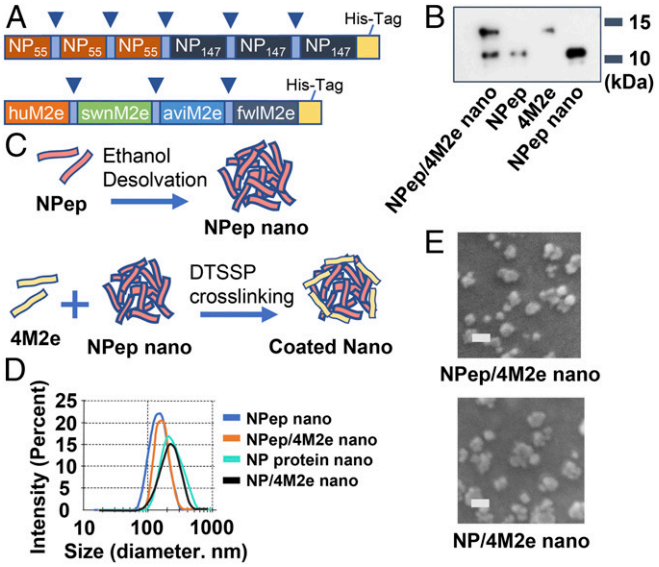

Fig. 1. Characterization of double-layered peptide nanoparticles. (*A*) Schematic diagram of the NP peptide (NPep) and 4M2e. 4M2e is composed of four tandem repeats of M2e epitopes connected with short flexible linker sequences (blue arrowheads). (*B*) Western blotting analysis of 4M2e, NP peptide, and nanoparticles using anti–His-tag monoclonal antibody. (*C*) Schematic diagram of core nanoparticle fabrication and double-layered nanoparticle generation. An additional layer of the 4M2e peptide was cross-linked onto the desolvated NP-peptide particulate core surface via DTSSP cross-linking. (*D*) Size distribution of NP-peptide nanoparticles (NPep nano), NP-peptide/4M2e–layered nanoparticles (NPep/4M2e nano), NP-protein nanoparticles (NP nano), and NP-protein/4M2e–layered nanoparticle NP/4M2e nano). (*E*) Scanning electron microscopy of NP-peptide/4M2e–layered nanoparticles and NP-protein/4M2e–layered nanoparticles. (Scale bars, 200 nm.)

We reduced cross-linked NP-peptide nanoparticles into single peptides and probed them with anti–His-tag monoclonal antibodies in a Western blot analysis (Fig. 1*B*). Band intensity analysis estimated the overall percentage of 4M2e in coatings to be 34.8% in NP-peptide/4M2e–layered nanoparticles (Fig. 1*B* and *SI Appendix*, Fig. S2*D*). The strong binding of both 4M2e-coated nanoparticles to an M2e monoclonal antibody (14C2) in sandwich ELISA confirmed the antigenicity of 4M2e in coatings of the layered nanoparticles (*SI Appendix*, Fig. S2*E*). NP-protein nanoparticles and NP-protein/4M2e–layered nanoparticles, but not NP-peptide nanoparticles and NP-peptide/4M2e–layered nanoparticles, can be captured by goat anti-mouse ribonucleoprotein (RNP) immune sera (*SI Appendix*, Fig. S2*F*), demonstrating that the NP peptide does not contain B cell antigens.

NP-Peptide/4M2e–Layered Nanoparticles Induced Robust Protective Immune Responses Against Reassortant H5N1 Infection in Mice. To evaluate the protective efficacy of the resulting nanoparticle vaccines, we IM immunized mice twice with a 4-wk interval in the absence of adjuvants (Fig. 2*A*). Strong IgG2a-biased seroconversion against M2e was elicited 3 wk after the boosting immunizations in both 4M2e-coated nanoparticle groups (Fig. 2 *B*–*D*). Immunization with a soluble peptide mixture of 35% 4M2e and 65% NP composite peptide induced ∼100-fold lower M2e-specific antibody titers than 4M2e-coated layered nanoparticles. Immunization with NP-peptide/4M2e–layered nanoparticles induced the

greatest IgG2a-biased antibody responses (Fig. 2*D*). The M2e antibodies induced by both types of the layered nanoparticles showed strong cross-reactivity to diverse M2e peptides, including human influenza M2e consensus, A/California/7/2009 (H1N1, p09) M2e, A/Vietnam/1203/2004 (H5N1, Vtn) M2e, and A/Shanghai/2/2013 (H7N9, SH) M2e (Fig. 2*E* and *SI Appendix*, Table S2). However, we did not observe a NP-specific antibody response from the NP-peptide/4M2e–layered nanoparticle group.

Both NP-peptide/4M2e– and NP-protein/4M2e–layered nanoparticles induced broad cellular responses and stimulated IFN-γ–secreting splenocyte populations (Fig. 3*A*). The NP-peptide/4M2e–layered nanoparticle group showed much higher levels of NP_{147}- and NP_{55}-specific IFN-γ–secreting splenocytes. In previous studies, peptide mixture reactivation of splenocytes indicated the successful induction of vaccine-specific cellular immune responses (34, 35). We measured levels of IFN-γ, IL-4, and IL-2 from the splenocyte culture medium in the presence of a peptide pool containing equal amounts of 4M2e and the NP peptide 3 wk after the boosting immunization. Both NP-peptide/4M2e and NP-protein/4M2e–layered nanoparticle-immunized groups showed elevated IFN-γ, IL-4, and IL-2 levels in the medium. Compared with the NP-protein/4M2e–layered nanoparticle and the soluble peptide mixture groups, the NP-peptide/4M2e–layered nanoparticle group showed higher levels of IFN-γ and IL-2 but not IL-4 production from the splenocyte culture after the restimulation (Fig. 3 *B*–*D*).

To investigate the role of the nanoparticle motif in protection against influenza challenges, we included an ovalbumin (OVA) nanoparticle group in immunization experiments. The OVA nanoparticle group showed higher levels of IL-4 and IL-2 compared with the Dulbecco's PBS (DPBS) group (Fig. 3 *C* and *D*). The secretion levels of IFN-γ, IL-4, and IL-2 were undetectable in the bronchial alveolar lavages (BAL) in all groups 3 wk after the boosting immunization.

Prophylaxis potency was evaluated with mouse challenge studies. Four weeks after the boosting immunization, we used 6 × 50% mouse lethal dose (mLD_{50}) of mouse-adapted H5N1 (rVn, PR8 H1N1 backboned virus) for an intranasal (IN) challenge (27). Fig. 4 demonstrates that both types of layered nanoparticle vaccination completely protected mice against death. However, NP-peptide/4M2e–layered nanoparticle-immunized mice experienced a faster recovery than NP-protein/4M2e–layered nanoparticle-immunized mice (Fig. 4*A*). Mice in the OVA nanoparticle group did not survive the challenge and experienced a similar weight loss as those in the DPBS group. The soluble peptide mixture immunization slightly delayed mortality, but mice in this group perished at day 10 after the infection (Fig. 4*B*).

NP-peptide/4M2e–layered nanoparticle immunization reduced mouse lung viral titers at day 5 after the infection compared with the mock-immunization or soluble peptide mixture immunization (*SI Appendix*, Fig. S3*A*). Histological analysis showed decreased leukocyte infiltration in the lungs of NP-peptide/4M2e–layered nanoparticle-immunized mice (*SI Appendix*, Fig. S3 *B* and *C*). This diminished proinflammatory response is consistent with the improved protection observed in the challenge studies.

Next, we tested whether the stability of the NP-peptide/4M2e–layered nanoparticles is independent of refrigeration by evaluating the M2e antigenicity of NP-peptide/4M2e–layered nanoparticles. The nanoparticles were preserved for different periods (20, 40, and 60 d of storage) at different temperatures (4 °C and 25 °C). ELISA results showed that these layered nanoparticles retained their antigenicity for 60 d at 25 °C (*SI Appendix*, Fig. S4*A*).

We also evaluated the M2e-specific immunogenicity of the layered peptide nanoparticles that were stored for 60 d at 4 °C or 25 °C versus freshly fabricated nanoparticles in mouse immunization experiments. We immunized naïve BALB/c mice with the same prime/boost regimen as described in Fig. 2*A*. Antibody titration results revealed an insignificant decrease in M2e-binding antibody titers induced by nanoparticles stored at 25 °C compared with 4 °C (*SI Appendix*, Fig. S4*B*). However, the freshly fabricated nanoparticles induced significantly higher M2e-binding antibody titers than nanoparticles stored at 25 °C, demonstrating that a 60-d preservation at 25 °C (but not 4 °C) decreased the immunogenicity of NP-peptide/4M2e–layered nanoparticles.

Antibodies and $CD8^+$ T Cells Correlated with Immune Protection. We investigated the effector mechanisms of immune protection and found that stronger cellular immune responses correlated with faster recovery after lethal viral infections (Figs. 3*A* and 4*A*). We

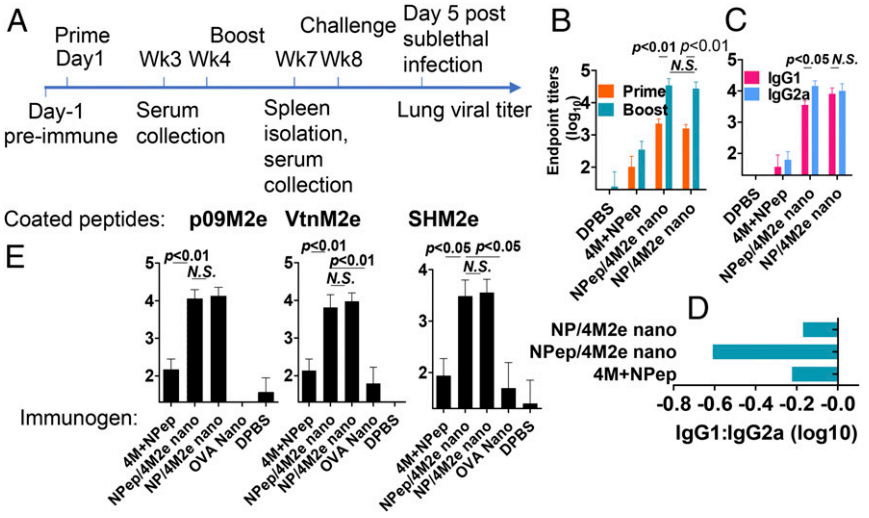

Fig. 2. Humoral immune responses induced in immunized mice. (*A*) Immunization and challenge experiment timeline. Immunization groups include soluble peptide mixture of 4M2e and the NP peptide (4M+NPep), NP-peptide/4M2e–layered nanoparticles (NPep/4M2e nano), NP-protein/4M2e–layered nanoparticles (NP/4M2e nano), OVA nanoparticles (OVA nano) and DPBS. (*B*) M2e-specific IgG endpoint titers. IgG titers against 4M2e were determined with serum samples collected 3-wk postboosting. (*C*) Determination of IgG1 and IgG2a titers against 4M2e using ELISA. (*D*) Bar chart showing logarithm values of the ratio IgG1:IgG2a. (*E*) M2e binding spectrum. Serum IgG binding capacity to various M2e peptides, including p09M2e, VtnM2e, and SHM2e was evaluated. Data are presented as mean ± SD (n = 10). Statistical significance was analyzed by t test for *B*, *C*, and *E*. P values shown in bar charts and N.S. indicates no significance between two compared groups. The experiments were repeated twice with the same samples with similar results.

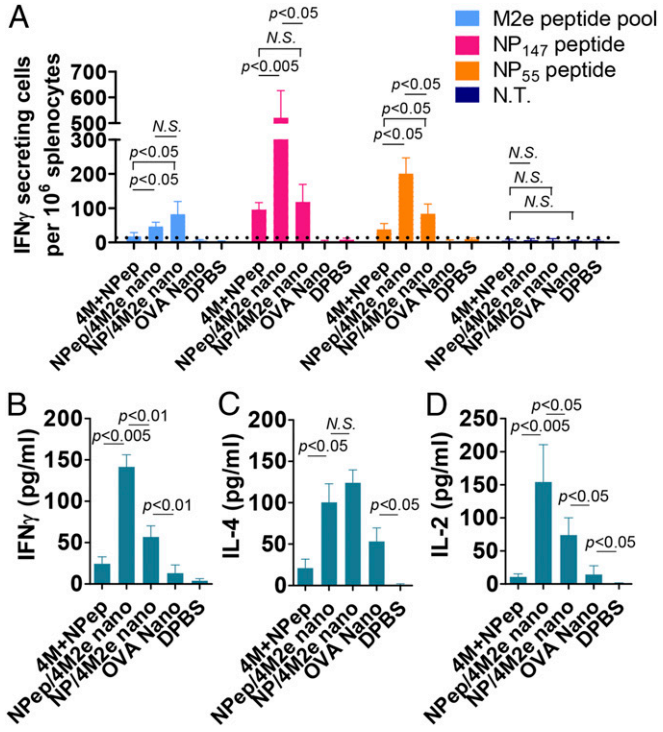

Fig. 3. Cellular immunity. (*A*) Cellular immune response specific to M2e, NP_{147}, and NP_{55}. Peptide pool-stimulated IFN-γ–secreting cell clones were determined using ELISpot assay ($n = 4$). (*B–D*) Splenocyte cytokine secretion. Lymphocytes from immunized mouse spleens were stimulated with a peptide mixture containing 4M2e and NP peptides. The levels of secreted cytokines including IFN-γ (*B*), IL-4 (*C*), and IL-2 (*D*) in the splenocyte culture medium were tested with cytokine ELISA. Data are presented as mean ± SD ($n = 3$). Statistical significance was analyzed by *t* test. *P* values shown in bar charts and N.S. indicates no significance between two compared groups. The experiments were repeated twice with the same samples with similar results.

investigated the roles of $CD4^+$ and $CD8^+$ immune cells in providing protection by applying depleting antibodies before 6 × mLD_{50} H5N1 rVn challenge in IM immunized mice. The results demonstrated that the $CD8^+$ cell depletion, but not the $CD4^+$ cell depletion, diminished the immune protective efficacy (Fig. 5 *A* and *B*). The mock-vaccinated mice (negative controls) died at day 9 after the challenge (Fig. 5*B*).

Next, we passively transferred immune sera from the NP-peptide/4M2e–layered nanoparticle group or preimmune sera to two groups of naïve mice ($n = 5$). After 24 h, mice were IN challenged with 6 × mLD_{50} H5N1 rVn virus (Fig. 5 *C* and *D*). In contrast to the mice receiving the preimmune sera, 60% of the mice receiving the immune sera survived the challenge, indicating serum antibodies played a role in the immune protection conferred by the layered peptide nanoparticle immunization.

We also observed that NP-peptide/4M2e–layered nanoparticle immune sera strongly bound H5N1 rVn-infected Madin-Darby canine kidney (MDCK) cells using immunofluorescence microscopy (Fig. 5*E*). However, we did not detect a viral neutralization effect (Fig. 5*F*). Fc-mediated effector mechanisms, such as antibody-dependent cellular cytotoxicity (ADCC), contribute to protection against influenza challenges (36, 37). Fig. 5*G* shows that NP-peptide/4M2e–layered nanoparticles induced nonneutralizing antibodies with ADCC potency against M2-expressing cells.

Nanoparticle Antigen Depot Effect Contributed Relatively Long-Lasting Antigen Presentation and Processing in Secondary Lymphoid Organs. We validated the robust power of particulate antigens in enhancing an antigen's immunogenicity, as described above. JAWS-II dendritic cells more effectively took up desolvated nanoparticles in vitro (compared with soluble antigens) (*SI Appendix*, Fig. S5*A*), which stimulated greater TNF-α secretion (*SI Appendix*, Fig. S5*B*).

Using in vivo imaging, we analyzed the transport kinetics of desolvated nanoparticles and soluble antigen molecules. We fluorescently labeled a representative influenza H7N9 HA (H7) and desolvated the labeled H7 into nanoparticles (16). The resulting nanoparticles showed an average hydrodynamic diameter of 214 ± 73 nm (Fig. 6*A*), which is comparable to the NP-peptide/4M2e–layered nanoparticles. We investigated the in vivo biodistribution using an in vitro imaging system (IVIS) (Fig. 6*B*). The radiant efficiency at the injection site of the nanoparticles did not decline for 48 h after the injection, but that of soluble antigens decayed in the same period, demonstrating the strong antigen depot effect of nanoparticles. Five days after the injection, the radiant efficiency of nanoparticles was still seen, while the radiant efficiency of the soluble proteins decreased to baseline levels (Fig. 6*C*). Because of the low detection of in vivo fluorescent signals, we isolated the draining lymph organs, the inguinal lymph nodes (iLN), and spleens for IVIS imaging at day 8 after the injection (Fig. 6*D*). The iLNs and spleens from mice receiving the nanoparticles showed significantly stronger radiant signal than those receiving the soluble protein or from naïve mice (Fig. 6 *E* and *F*).

Supplementation with NP-Peptide/4M2e–Layered Nanoparticles Improved Heterosubtypic Protection of Inactivated Influenza Vaccines. We previously found that codelivery of inactivated influenza vaccines with a flagellin–M2e fusion protein by dissolvable MN patches can broaden the protective efficacy of inactivated influenza vaccines (38). Next, we investigated if the peptide nanoparticles will also synergize with inactivated influenza vaccines to induce stronger cross protection. We coadministered NP-peptide/4M2e–layered nanoparticles with inactivated PR8 either IM or via the skin by a MN patch. Our results showed around 70% delivery efficacy via MN patches after extending the insertion time to 20 min, and that the nanoparticle dose administered was 5.3 μg by one MN patch. After the immunization, most of the MNs were fully dissolved (*SI Appendix*, Fig. S6*A*). Upon insertion into mouse skin, the MNs penetrated to a depth corresponding to the thickness of the epidermis and upper dermis layers (~100–200 μm) (*SI Appendix*, Fig. S6*B*), which does not cause pain but facilitates antigen uptake by Langerhans cells (39).

Serum antibody titers were measured 3 wk after the boost. Coadministered NP-peptide/4M2e–layered nanoparticles in either the IM or MN route enhanced anti-PR8 HA inhibition (HAI) titers at similar levels (Fig. 7*A*). Both M2e-specific IgG1 and IgG2a were significantly induced (Fig. 7*B*). NP-peptide/4M2e–layered nanoparticle immunization alone induced an IgG2a-biased antibody response but the addition of inactivated PR8 converted

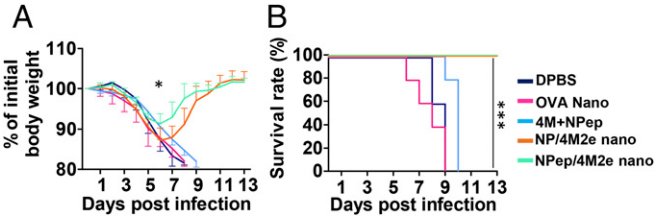

Fig. 4. Virus challenge with reassortant H5N1 rVn. (*A*) Morbidity. (*B*) Mortality. IM immunized BALB/c mice were challenged with lethal dose 6 × mLD_{50} rVn. Error bars represent mean ± SD. The difference in weight loss between NP-protein/4M2e–layered nanoparticle (NP/4M2e nano) and NP-peptide/4M2e–layered nanoparticle (NPep/4M2e nano) groups was analyzed by two-way ANOVA and *P* value was shown in morbidity curves. The statistical analysis of survival rate difference between the mixture of 4M2e and NP peptides and NP-peptide/4M2e–layered nanoparticle groups was performed with a log-rank test (*$P < 0.05$; ***$P < 0.005$, $n = 5$).

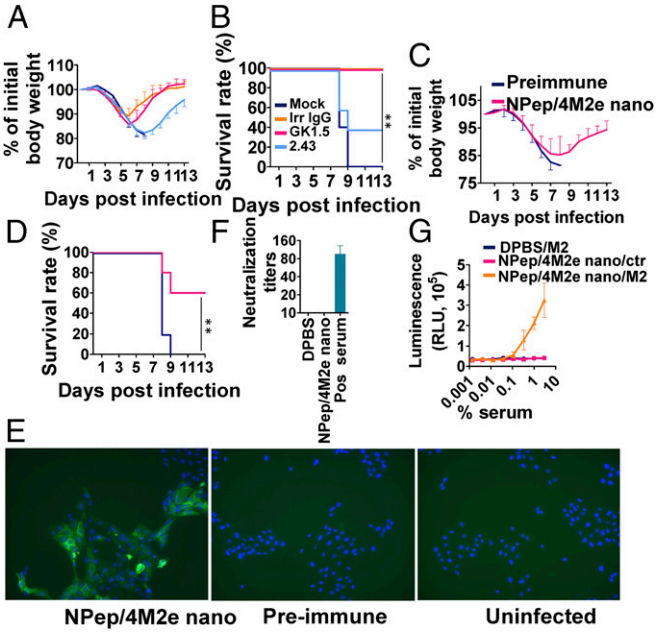

Fig. 5. Protective mechanisms. (*A*) Morbidity and (*B*) mortality of clone GK1.5-treated $CD4^+$-depleted or clone 2.43-treated $CD8^+$-depleted BALB/c mice that were IM immunized twice were evaluated after lethal dose 6 × mLD_{50} infection with H5N1. Antiflagellin IgG1 clone X5A12 was used as an irrelevant negative control, and DPBS was used for mock-treatment. ($n = 5$) (*C*) Morbidity and (*D*) mortality of serum passively transferred BALB/c mice were evaluated after lethal dose 6 × mLD_{50} infection with H5N1 ($n = 5$). (*E*) Immunofluorescence staining of H5N1-infected MDCK cells using preimmune and NP-peptide/4M2e–layered nanoparticles (NPep/4M2e nano) immune serum as the primary antibodies and then Alexa Fluor 488 Goat Anti-Mouse IgG as the secondary antibody. The uninfected MDCK cells incubated with NP-peptide/4M2e–layered nanoparticle immune serum were the negative control. (Magnification, 10× objective.) (*F*) Viral neutralization potency of immune sera was evaluated in a standard neutralization assay against H5N1. Convalescent mouse serum from H5N1-infected mice was used as a positive control. (*G*) ADCC surrogate assay with pooled pre-challenge sera from NPep/4M2e–layered nanoparticle and DPBS immunization groups and HEK293T cells stably expressing M2. The nontransfected HEK293T cells were used as the negative control ($n = 3$). Data are presented as mean ± SD. Statistical significance was analyzed by *t* test for *F* and *G*. *P* values shown in bar charts and N.S. indicates no significance between two compared groups. The statistical analysis of survival rate difference between the antibody-treatment group and the mock-treatment group in *B* and *D* was performed with a log-rank test (**$P < 0.01$; $n = 5$). The experiments of (*E*) immunofluorescence staining and (*F*) viral neutralization assay were repeated twice with similar results.

the M2e-specific antibody response to an IgG1-bias regardless of the IM or MN route (Fig. 7*C*).

We evaluated the protective efficacy of different immunizations by challenge experiments with a lethal dose of 6 × mLD_{50} PR8 H1N1 or A/Philippines/2/1982 (Phi) H3N2. Immunization with inactivated PR8 alone provided only homologous protection but coimmunization with the inactivated PR8 and NP-peptide/4M2e–layered nanoparticles through either the IM or MN route protected mice against homologous and heterosubtypic viral challenges (Fig. 7 *D* and *E* and *SI Appendix*, Fig. S7 *A* and *B*). The two routes were comparable in inducing immune protection.

Mice immunized with inactivated PR8, with or without an addition of NP-peptide/4M2e–layered nanoparticles, cleared lung viruses by day 5 after a sublethal infection of 0.5 × mLD_{50} PR8 (*SI Appendix*, Fig. S7*C*). Immunization with NP-peptide/4M2e–layered nanoparticles alone significantly reduced lung viral titers compared with the DPBS negative group. The addition of NP-peptide/4M2e–layered nanoparticles to inactivated PR8 also reduced heterosubtypic lung viral titers at day 5 after a sublethal infection of 0.5 × mLD_{50} Phi (*SI Appendix*, Fig. S7*D*).

MN Patch Delivery Conferred Strong Long-Term Immunity. To assess the longevity and efficiency of recall responses in mice, we investigated the immune responses 12 wk after the boosting immunization by MN or IM administration and the capacity to clear influenza virus from the lung 13 wk after the vaccination. Unlike immunization with inactivated PR8 alone, coimmunization of inactivated PR8 with NP-peptide/4M2e–layered nanoparticles maintained the anti-PR8 HAI titer levels for 12 wk after the boosting immunization (Fig. 8*A*) and induced robust M2e-specific serum IgG titers (Fig. 8*B*). Furthermore, the coimmunization group increased the levels of M2e-specific IgG from BAL 12 wk after the boosting immunization (Fig. 8*C*). M2e-specific IgA titers from BAL were undetectable at weeks 3 and 12 after the immunization.

We IN infected mice with a sublethal dose of 0.5 × mLD_{50} Phi at week 13 after the boost. On day 5 after the infection, the IM coimmunized group showed a lung viral titer 40-fold lower than

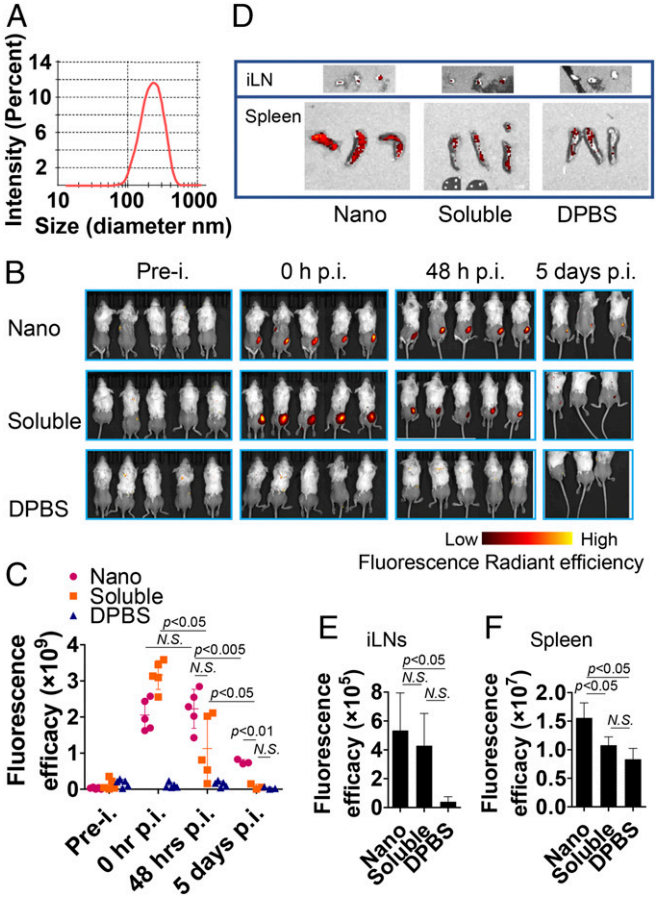

Fig. 6. In vivo visualization in mice. (*A*) Size distribution of fluorescent H7 nanoparticle. (*B*) Biodistributions of IM injected Alexa Fluor 700 succinimidyl ester dye-conjugated fluorescent H7 nanoparticle and fluorescent soluble H7 protein were analyzed in vivo using Perkin-Elmer IVIS Spectrum In Vivo Imaging System at the following time points: preinjection (prei.), 0-h postinjection (hpi), 48 hpi, and 5 dpi. Mice injected with DPBS were used as negative controls. (*C*) Fluorescence radiant efficiency in vivo was quantified at the indicated four time-points in *B* using Living Image software. (*D*) Biodistributions of fluorescent H7 nanoparticle and fluorescent soluble H7 protein in iLN and spleens were analyzed at 8 dpi. The iLN and spleens isolated from DPBS-injected mice were used as negative controls. Fluorescent radiant efficiency in (*E*) iLN and (*F*) spleens were quantified 8 dpi using Living Image software. Data are presented as mean ± SD. Statistical significance was analyzed by two-way ANOVA for *C* and by *t* test for *E* and *F* *P* values shown in bar charts and N.S. indicates no significance between two compared groups.

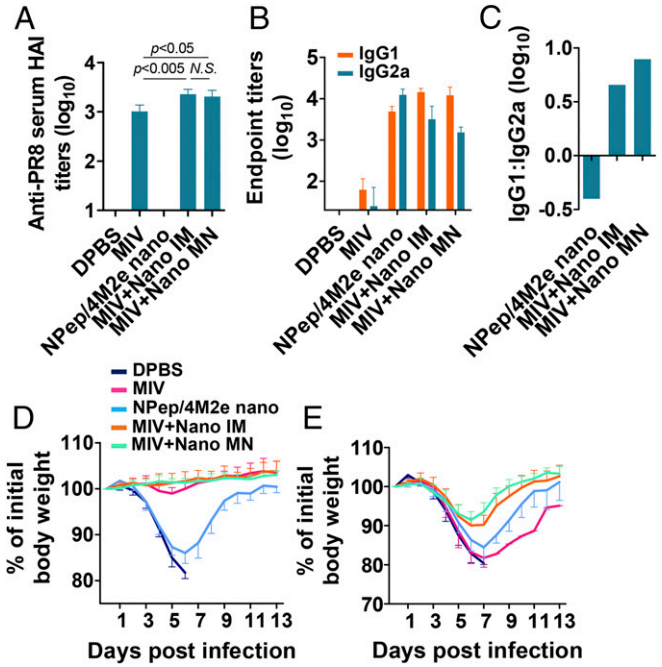

Fig. 7. Immunity induced by supplementation of monovalent inactivated PR8 vaccine (MIV). IM immunization groups include 10 μg NP-peptide/4M2e–layered nanoparticles (NPep/4M2e nano), 10 μg MIV, 10 μg MIV plus 7.5 μg NP-peptide/4M2e–layered nanoparticles (MIV+Nano IM), 10 μg MIV plus MN patch containing 7.5 μg NP-peptide/4M2e–layered nanoparticle (MIV+Nano MN), or 50 μL DPBS as a placebo. (*A*) Anti-PR8 serum HA inhibition titers of serum collected 3-wk postboosting immunization ($n = 5$). (*B*) Determination of IgG1 and IgG2a titers against M2e using ELISA method ($n = 8$). (*C*) Bar chart showing logarithm values of the ratio IgG1: IgG2a. Morbidity of immunized BALB/c after lethal dose 6 × mLD_{50} infection with PR8 (*D*) and Phi (*E*). Data are presented as mean ± SD in *A*, *B*, *D*, and *E*. Statistical significance was analyzed by *t* test for *A*. *P* values shown in bar charts and N.S. indicates no significance between two compared groups.

mock-immunized infected mice. MN patch coimmunized mice showed a lung viral titer 433-fold lower than the mock-immunized mouse lung viral titer (Fig. 8*D*). Furthermore, MN patch coimmunized mice showed more robust recall responses than IM coimmunized mice, as shown by more efficient virus clearance.

Next, we investigated the induction of cellular immune responses upon sublethal challenge with Phi 13 wk after the boosting immunization. We restimulated splenocytes isolated from challenged mice on day 5 with the NP-peptide and 4M2e mixture for 72 h. The MN immunization group exhibited the highest recall cytokine production of IL-4 and IFN-γ at day 5 after the infection (Fig. 8*E*).

Antibody-secreting cells (ASCs) are partly responsible for recall immune responses that confer protection against influenza infection. We determined M2e-specific IgG ASCs in isolated splenocytes on day 5 after infection. Fig. 8*F* shows that both IM and MN groups had significantly elevated ASC numbers compared with the mock- or inactivated PR8-immunized group.

Discussion

We fabricated NP-peptide/4M2e–layered nanoparticles approximately the size of influenza A virions with a core of NP peptides and a coating of conserved 4M2e peptides. This approach produced peptide nanoparticles comprised almost entirely of the peptide antigens of interest. We have found that the core immunogen preferentially induces cellular immunity while the coating immunogen preferentially induces humoral immunity. We speculate that this immunogenic feature is a benefit of the layered architecture and physiologically activated disassembly of the layered nanoparticles. Naïve B cells can directly recognize and be activated by the coating immunogen of the nanoparticle. As well, once endocytosed by an APC, the core immunogen is released from the nanoparticles and processed and presented on MHC class molecules. Furthermore, the nanoparticles have an immunogen depot effect that keeps them concentrated in draining lymph nodes for a longer period than soluble protein/peptide antigens. The results of the present study provide insights into this effective format of particulate influenza vaccine.

We have explored the influence of various parameters on nanocluster size, including desolvent addition speed, desolvent exposure time, salt concentration, cross-linker type, cross-linking time, and other factors (40, 41). Others have shown batch-to-batch reproducibility of the synthesis process, with initial pH being an important factor in nanoparticle formation (42, 43). The primary factors governing nanoparticle formation are solvent–protein, solvent–desolvent, and desolvent–protein interactions. We and others have also reported on multiple solvent-desolvent combinations for nanoparticle synthesis (44, 45). Von Storp et al. (44) in particular found desolvent composition can adjust the nanoparticle size range between 50 and 300 nm. Our previous study showed significant changes in the nanoparticle size to some factors in the fabrication process, such as

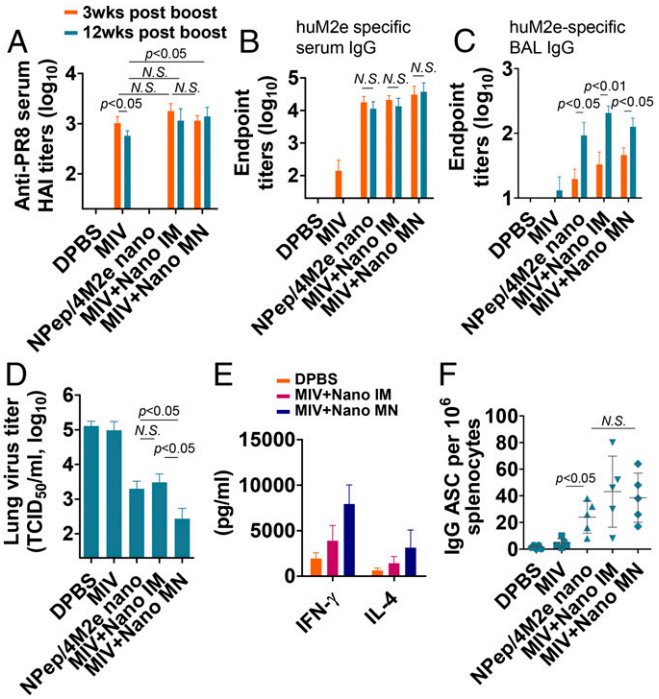

Fig. 8. Long-term immunity induced by MN patch skin vaccination. (*A*) Anti-PR8 serum HA inhibition titers of serum collected 3- and 12-wk postboosting ($n = 5$). Serum IgG (*B*) and BAL IgG (*C*) titers against huM2e were determined with serum samples collected 3- and 12-wk postboosting. (*D*) Lung physiology in virus challenge infection. Determination of mouse lung virus titers at day 5 after a sublethal dose 0.5 × mLD_{50} infection with Phi ($n = 3$). (*E*) and (*F*) To determine systemic cellular immune responses, splenocytes were isolated at 5 d after sublethal dose 0.5 × mLD_{50} infection with Phi. (*E*) IFN-γ and IL-4 levels in 4M2e and NP-peptide–reactivated splenocytes culture medium were determined via cytokine ELISA ($n = 5$). (*F*) 4M2e-specific IgG antibody-secreting cells from recalled splenocytes were analyzed using ELISpot ($n = 5$). Data are presented as mean ± SD. Statistical significance was analyzed by *t* test. *P* values shown in bar charts and N.S. indicates no significance between two compared groups. The experiments of anti-PR8 serum HA inhibition titration assay (*A*), serum IgG (*B*), and BAL IgG (*C*) titration assays were repeated twice with similar results.

the cross-linker concentration and protein materials (but not desolvation ratio) (27).

Desolvent choice also influences the nanoparticle size. While we initially chose ethanol for its limited toxicity, others have found that desolvation with methanol and ethanol blends can produce nanoclusters in the sub 100-nm range, while blends of ethanol and acetone increase the particle size into the 140- to 300-nm range (44). Isopropanol is another solvent commonly used for desolvation (46). We have also performed experiments using different desolvation reagents (ethanol, methanol, or isopropanol) at the same desolvation ratio (solvent:solution 4:1) to desolvate NP peptide, recombinant M2e-NA tetramer protein, or OVA into nanoparticles. The results indicated that there were no significant differences in nanoparticle size after applying the different desolvents to the same protein sample.

An ideal universal influenza A vaccine should induce heterosubtypic immunity that can protect against challenges by viruses from different influenza A subtypes. Clinical trials have proven the immunogenic potential of some NP- and M2e-based influenza vaccine candidates (8, 47, 48). We opted to use peptides because peptide immunogens are less likely to induce allergic or autoimmune responses due to the lack of redundant components that might cause antigen mimicry between pathogen and human proteins (49). Because our peptides include known specific epitopes only (MHC-I–restricted epitope NP_{147} and MHC-II–restricted epitope NP_{55}), the resulting peptides can induce $CD8^+$ CTL and $CD4^+$ Th-1 responses. However, as proven by many studies, minimal antigenic epitopes are often poorly immunogenic (50).

The low immunogenicity of small peptides can be overcome by using some sort of vector or platform for the peptides. Liposomal and poly(lactic-co-glycolic-acid) (PLGA) nanoparticles loaded with two synthetic peptides (17 and 24 amino acids in length) have efficiently induced functional T cell responses (51). In comparison, immunizations with the NP-peptide/4M2e–layered nanoparticles induced robust IgG2a-biased cross-reactive anti-M2e antibody responses and T cell responses against NP_{147} and NP_{55}. The induced immunity fully protected mice against lethal homologous and reassortant H5N1 rVN (27) viral challenges, demonstrating the potential of layered peptide nanoparticles in overcoming peptide antigens' low immunogenicity. M2e-specific antibody titers induced by NP-peptide/4M2e–layered nanoparticles were similar to that of headless HA-coated 4M2e protein nanoparticles, but 2.5-fold lower than that of the uncoated 4M2e protein nanoparticle (27). We speculate that this decrease in titers correlates to the coating efficacy and monomeric state of 4M2e peptide on the NP-peptide/4M2e–layered nanoparticle surface. The monomer of 4M2e is known to be less immunogenic than the tetramer (52).

The difference between the in vivo transport kinetics of the nanoparticles and the soluble peptide antigens correlated to the enhanced nanoparticle immunogenicity. Efficient draining of nanoparticles to lymphoid tissues, prolonged tissue residence, and controlled release of antigens and adjuvants enhances the immunity achieved (53). Ultrasmall nanoparticles less than 10 nm in diameter or soluble antigenic molecules can rapidly diffuse into and out of lymph organs, thus decreasing the opportunity of APCs' uptake (54). In the present study, nanoparticles around 200 nm were efficiently drained to iLN and spleens and retained there for a relatively long period, increasing the chance to be presented by APCs. The soluble molecules diffused rapidly from the injection sites and disappeared earlier from the lymph nodes. The entrapment in immune tissues, resistance to degradation, and intracellularly activated disassembly of nanoparticles within APCs allow for the sustained processing and releasing of peptides for a longer period versus soluble antigens, potentially shaping memory T cells and long-term immunity (55). The layered nanoparticles overcame the weak immunogenicity of peptide antigens through the aforementioned mechanisms.

Dissolvable MN patch-based skin vaccination has enhanced the immunogenicity of influenza vaccines (56–59). MN patch vaccination with inactivated influenza virus resulted in more efficient lung virus clearance and enhanced cellular recall responses than IM vaccination after influenza challenge (57). Our results demonstrated that the MN patch skin vaccination is superior to the IM route in inducing long-lasting immune responses (38). Additional benefits of encapsulating nanoparticles in MN patches include less dependence on the cold-chain in vaccine transportation, increased acceptability and accessibility, and self-administration (58).

Layered peptide nanoparticles have great potential for commercial production. Without a need for glycosylation, not only can *Spodoptera frugiperda* Sf9 cells (Sf9) insect cell expression systems or *Escherichia coli* expression systems produce the NP peptide but also chemical synthesis in a large scale is also possible. As described in *Materials and Methods*, the double-layered nanoparticle fabrication process is inexpensive without the need for special production systems. We have found in some cases >90% yield on protein or peptide incorporation into nanoparticles (40). While the synthesis process needs to be optimized for each new type of protein or peptide, it is feasible to get very high nanoparticle yields from this process by a further parameter optimization. Additionally, ethanol as a relatively nontoxic desolvent for nanocluster synthesis makes the synthesis process more amenable to safe, large-scale production.

Maintenance of proper mixing is also essential during the scale-up of any process, and improper mixing during desolvation can lead to a more heterogeneous size distribution of particles (60). A recent study showed that increasing stirring speed and changing impeller shape could maintain proper mixing of desolvated gelatin nanoparticles in gram-scale batches (61). Furthermore, we showed that ultrafiltration was a viable, commercially relevant alternative to particle collection by centrifugation (62).

With appreciated antigen distribution properties, intracellularly controlled release, simple manufacture processes, and robust thermostability, we foresee layered peptide nanoparticles having a broad utilization in peptide vaccines and peptide drug delivery.

Conclusion

In summary, we utilized molecular biology techniques to generate composite peptides containing known epitopes, fabricated peptide-based nanoparticles, and demonstrated the proof-of-concept of a universal influenza vaccine. To broaden the application of our double-layered nanoparticle fabrication method in vaccine design, we can cross-link conformational B cell epitopes [such as headless HA (27) or neuraminidase] into the coating layer. The successful combination of peptide nanoparticles with dissolvable MN patches demonstrated a potential alternative to conventional IM needle-syringe injection. Further study to map human CTL epitopes in NP and other internal proteins should provide clues for designing better T cell epitope-based nanoparticles for human vaccination.

Materials and Methods

Ethics Statement. We carried out this study in strict accordance with the recommendations in the *Guide for the Care and Use of Laboratory Animals* of the National Institutes of Health (63). All animal studies were approved by the Georgia State University Institutional Animal Care and Use Committee (IACUC) under protocol no. A16024. Female BALB/c mice (6- to 8-wk-old) were purchased from Jackson Laboratory and were housed in the animal facility at Georgia State University. Bleeding, infection, and sampling were performed under light anesthesia via inhalation of isoflurane to reduce mouse suffering.

Design of Peptides 4M2e and NP Peptide. The encoding gene of peptide 4M2e was generated by primer extension with overlapping PCR. GenScript synthesized the gene encoding the NP epitope composite peptide. A signal peptide encoding sequence from honey bee melittin was employed in both 4M2e and NP peptide constructs to facilitate expression and secretion in

insect Sf9 (ATCC, CRL-1711). A six-histidine-tag sequence was added after the 4M2e and NP peptide sequences. *SI Appendix*, Table S2 and Fig. 1*A* list the four copies of different M2e sequences and their order in 4M2e. *SI Appendix*, Notes S1 and S2 and Fig. 1 present a list of the nucleotide sequence, amino acid sequence, and order of tandem copies of NP epitopes in the composite peptide construct. Molecular evolutionary genetics analysis v6.0 (MEGA6) and Microsoft Excel were used to align and analyze sequences. The 4M2e and NP peptides were purified from recombinant baculovirus-based protein expression in insect cells.

Nanoparticles Fabrication. Peptide nanoparticles were made as previously described with modification (27). NP epitope composite peptide or the NP protein (Cat no. 40207-V08B; Sino Biological) solution in DPBS (Thermo Scientific) was desolvated with a 4:1 volume ratio of absolute ethanol to the peptide or protein solution. The desolvated nanoparticle pellets were resuspended by sonication in either 4M2e in DPBS, or DPBS. Generated nanoparticles included NP-peptide/4M2e–layered nanoparticles, NP-protein/4M2e–layered nanoparticles, NP-peptide nanoparticles (without a coating layer), and NP-protein nanoparticles (without a coating layer). The structures of the nanoparticles were stabilized and cross-linked by DTSSP. The fabrication of OVA protein nanoparticles was as described previously (40).

MN Patch Fabrication. MN patch fabrication has been previously described (59). Briefly, a casting solution containing 1 wt% polyvinyl alcohol, 10 wt% sucrose, and 7.5 μg of nanoparticles was cast onto a polydimethylsiloxane MN mold and allowed to dry to form the MNs. A second solution containing 18 wt% polyvinyl alcohol and 18 wt% sucrose was then cast and allowed to dry to form the MN patch backing. The MN patch was removed from the mold and stored with desiccant until use.

Nanoparticle Characterization. We assessed nanoparticle size distribution by dynamic light scattering with a Malvern Zetasizer Nano ZS (Malvern Instruments).

Peptide/protein concentration in the nanoparticle solution was assessed with a BCA assay per the manufacturer's instructions (Thermo Scientific).

NP-peptide/4M2e– and NP-protein/4M2e–layered nanoparticles were resuspended in water, air-dried, and sputter-coated with carbon before visualization with a Zeiss LEO 1450vp scanning electron microscope (Carl Zeiss) at 5.0 kV.

Antigen content of nanoparticles was analyzed in Western blots using anti–His-tag monoclonal antibody at 1 μg/mL (Product No. MA1-21315; Thermo Fisher Scientific).

Pull-Down Assay. The pull-down experiment was performed with Dynabeads Protein G (Cat no. 10003D; Thermo Fisher Scientific) according to the manufacturer's instructions, as described previously (27). The collected prewash, unbound fraction, and eluent samples were immediately analyzed using Western blot with 4 μg/mL rabbit anti-His polyclonal antibody (Cat no. PA1-983B; Thermo Fisher Scientific) for blotting.

ELISA. We tested the binding of nanoparticles to 14C2 or anti-RNP serum using a sandwich- ELISA method described previously (27).

In 100-ng/μL 14C2-coated 96-well Nunc-immuno MicroWell solid plates (Thermo Scientific), 50 μL of 1:3 serially diluted 4M2e-coated and uncoated nanoparticles were added for binding. A fusion protein FliC–4M2e (38) was used as a positive control. A monoclonal anti–His-tag antibody conjugated with horseradish peroxidase (HRP) (Cat no. R931-25; Thermo Scientific) was used as the detection antibody.

In goat anti-RNP serum- (Cat no. NR-3133; BEI Resources, NIH) coated plates, the antigenicity of 4M2e-coated and uncoated nanoparticles, NP protein (positive control; Cat no. 40207-V08B; Sino Biological), and FliC–4M2e (negative control) was measured. HRP-conjugated rabbit anti-goat secondary antibody (Cat no. 31402; Thermo Scientific) was used as detection antibody.

Serum antibody titers were analyzed using an ELISA method described previously (27).

Immunofluorescent Staining. MDCK cells were seeded at 5×10^4 cells per well in a 96-well black/clear polystyrene high-content imaging plate with a flat bottom (Cat. no. 353219; BD Falcon). The MDCK cells were then mock-infected or infected with rVn H5N1 at a multiplicity of infection of 0.5 in serum-free medium. After 1 h of incubation at 37 °C, the cells were washed three times with DPBS and incubated with a serum-free and trypsin-free medium for 48 h at 37 °C. The cells were then washed with DPBS and fixed with 1% paraformaldehyde at room temperature for 30 min. Cells were blocked with 5% milk solution in DPBS for 1 h at room temperature and stained at room temperature for 2 h with 1/300 diluted pooled preimmune sera or with serum from mice immunized with NP-peptide/4M2e–layered nanoparticles. Alexa Fluor 488 Goat Anti-Mouse IgG (Cat no. R37120; Thermo Fisher Scientific) was used as the fluorescently labeled secondary antibodies. The samples were visualized using a fluorescent microscope BZ-X710 (Keyence).

Immunization and Influenza A Virus Challenges. Mice (BALB/c strain, female, 6- to 8-wk-old) received IM immunizations twice, at a 4-wk interval, in the hind leg with 50 μL of one of the following vaccine mixtures in DPBS: 10 μg NP-peptide/4M2e–layered nanoparticles, 10 μg NP-protein/4M2e–layered nanoparticles, a peptide mixture containing 3.5 μg 4M2e and 6.5 μg NP-peptide, or 10 μg OVA protein nanoparticles. Fifty microliters of DPBS was used as a placebo. Blood samples were collected 2 d before the prime, 3 wk after the prime, and 3 wk after the boost. Four weeks after the boosting immunization, mice were challenged IN with $6 \times mLD_{50}$ of mouse-adapted influenza A virus strains in 50 μL DPBS. The strain used for the challenge was rVn H5N1 [rVn; HA and neuraminidase (NA) genes were derived from H5N1 (A/Vietnam/1203/2004), and the remaining backbone genes from PR8 H1N1] (27).

In the supplemental immunization experiment, mice received IM immunizations twice at 4-wk intervals, with 50 μL of one of the following vaccine mixtures in DPBS: 10 μg NP-peptide/4M2e–layered nanoparticles, 10 μg monovalent inactivated influenza virus (MIV), 10 μg MIV plus 7.5 μg NP-peptide/4M2e–layered nanoparticles, 10 μg MIV plus MN patch containing 7.5 μg NP-peptide/4M2e–layered nanoparticles, or 50 μL DPBS as a placebo. Four weeks after the boosting immunization, mice were challenged IN with $6 \times mLD_{50}$ of mouse-adapted influenza A virus strains in 50 μL DPBS. The strains used for challenges were PR8 H1N1 and A/Philippines/2/1982 (Phi) H3N2.

To determine long-term immunity, blood samples were collected 12-wk postboosting and immunized mice were challenged with $6 \times mLD_{50}$ mouse-adapted PR8 and Phi 13 wk after the boost.

To investigate the roles of activated T cells in immunoprotection, monoclonal antibodies were used for in vivo depletion of CD4 or CD8 T lymphocyte subsets using the method described previously (64). Depletion was accomplished by two intraperitoneal injections of 200 μg monoclonal antibodies 1 d before and 1 d after lethal dose $6 \times mLD_{50}$ infection with H5N1. Groups of mice ($n = 5$) were treated with clone 2.43 (Cat no. BE0061; BioXCell) for CD8 depletion, clone GK1.5 (Cat no. BE0003-1; BioXCell) for CD4 depletion, clone X5A12 anti-Flagellin FliC mouse IgG1 (Cat no. mabg-flic; Invivogen) as an irrelevant negative control, or DPBS as mock-treatment.

Body weight loss and survival rates were monitored daily for 14 d post-infection (dpi). Weight loss of ≥20% was used as the endpoint at which mice were killed per IACUC guidelines.

Evaluation of Mucosal and Systemic Cellular Immune Responses. We evaluated the number of IFNγ-secreting cells after restimulation using an enzyme-linked immunospot (ELISpot) method. Briefly, 3 wk after boosting, splenocytes were isolated from all immunization groups. Each well in a 96-well filtration plate (Catalog no. MSIPS4W10; Fisher Scientific) was loaded with 5×10^5 splenocytes for restimulation and a final concentration of 2 μg/mL of one of the following: an M2e peptide pool (comprised equal amounts of huM2e, p09, Vtn, and SH M2e peptides), NP_{147}-peptide, NP_{55}-peptide, or mock-restimulation. The developed plates were rinsed with purified water and air dried before being counted with a Bioreader-6000-E (Biosys). IFN-γ, IL-2, and IL-4 secretion levels from 4M2e and NP-peptide–reactivated splenocytes culture medium and BAL samples were measured using cytokine ELISA method.

To determine the long-term systemic cellular immunity, immunized mice were sublethally infected with $0.5 \times mLD_{50}$ Phi at 13-wk postboosting and splenocytes were isolated 4 d postinfection. IFN-γ and IL-4 secretion levels from 4M2e and NP-peptide–reactivated splenocytes culture medium were measured using cytokine ELISA.

IgG ASCs from splenocytes were measured using the modified ELISpot method. Briefly, 96-well plates were coated overnight at 4 °C with 4M2e peptide at a final concentration of 5 μg/mL. The plates were washed three times with RPMI 1640 (Cat no. 11875093; Gibco) and blocked for 2 h with 10% FBS before sample addition. Single-cell suspensions collected 4 dpi (1×10^6 cell in 100 μL per well) were plated directly on coated blocked plates and were incubated at 37 °C for 18 h. Plates were washed and then overlaid with HRP-conjugated anti-mouse IgG antibody for 1 h at room temperature. TrueBlue Peroxidase Substrate was added for spot detection. The spots were enumerated using a Bioreader-6000-E.

Determination of Lung Virus Titers. Three mice per immunization group were killed at day 5 after $0.5 \times mLD_{50}$ rVn, PR8, or Phi infection. Determination of lung virus titers was as described previously. The presence of virus in the

supernatant was assayed by measuring the HA activity in the supernatant, using the Reed and Muench method for calculation (65).

Histological Analysis. Three mice per immunization group were killed at day 5 after $0.5 \times mLD_{50}$ rVn infection. Lung tissues were isolated and fixed with 10% neutral buffered formalin for lung histological analysis, as described previously (27).

After applying MN patches on BALB/c mouse skin for 20 min, the immunized area of skin was removed and frozen in embedding medium (Tissue-Tek OCT Compound; Sakura Finetek) on dry ice for tissue cryo-sectioning. The randomly cut sections with 10-μm thickness were stained with H&E and examined microscopically.

Neutralization Assay. Pooled serum samples were heat-inactivated for 30 min at 56 °C. Mixtures of virus with final concentrations of $100 \times TCID_{50}$ virus per mixture and twofold serial diluted serum samples (final serum dilution from 1:10 to 1:1,280) were incubated for 2 h at 37 °C, 5% CO_2 in 50 μL virus medium (DMEM, 100 U/mL penicillin and 100 μg/mL streptomycin), then subsequently added to the MDCK cells and incubated for 72 h at 37 °C, 5% CO_2. A standard HA assay was performed to measure virus inhibition.

ADCC Surrogate Assay. An ADCC surrogate assay was performed according to the kit manufacturer's protocol (Cat no. M1211; Promega) with modification. Briefly, the M2-expressing MDCK cell culture medium was supplemented with 10 μM Amantadine (Sigma) to support cell growth, 7.5 μg/mL puromycin (Invitrogen), and 10% FBS at 37 °C, 5% CO_2. One day before the assay, M2-expressing MDCK cells were harvested and seeded in sterile white 96-well plates (Costar). After 24 h, serum samples were heat-inactivated for 30 min at 56 °C and then serially diluted in assay buffer [4% ultralow IgG FBS (Promega) in RPMI 1640 (Gibco)]. Serum dilutions and a stable Jurkat cell line-expressing mouse FcγRIV (Cat No. M1211; Promega) were added and incubated for 6 h at 37 °C at a target-effector ratio of 1:5. Cells were equilibrated to room temperature for 15 min before Bio-Glo Luciferase assay substrate (Promega) was added. Luminescence was read out after 10 min on a GloMax (Promega). Data are expressed as luminescence relative light units (RLU) of the signal in the absence of serum.

Tracking Fluorescent Nanoparticles in Vivo. To make fluorescent protein, 10 μL of 10 mg/mL Alexa Fluor 700 succinimidyl ester dye (Life Technologies) in DMSO was added to 50 μL of 5 mg/mL H7 protein in sterile 0.1 M sodium bicarbonate buffer (pH 8.3). The reaction was stirred at 800 rpm for 1 h at room temperature on a Thermo shaker (Grant Instruments), and excess dye was removed by buffer exchanging against over 100 volumes DPBS in a 3-kD diafiltration tube (Merck Millipore) until the filtrate was colorless.

Protein concentration was measured by BCA assay, and the conjugated dye concentration was measured by fluorescence against a standard curve of the free dye on a spectrophotometer (BioTek). To make fluorescent nanoparticles, 144-μg fluorescent H7 protein was added to 336-μg H7 protein (30% fluorescent H7 by mass) and used to create nanoparticles, as described above.

Mice to be given fluorescent proteins and nanoparticles were fed alfalfa-free diets for 2 wk before immunization to reduce background autofluorescence (LabDiet), and treated with a depilatory cream (Nair) around the injection site 1 d before immunization. Groups of five, 6- to 8-wk-old female BALB/c mice were injected with 10 μg of fluorescent H7 nanoparticles, 10 μg of fluorescent soluble protein mixing 30% fluorescent and 70% untreated soluble protein, or DPBS. Mice given fluorescent H7 nanoparticles, fluorescent soluble H7, or DPBS were used for in vivo antigen biodistribution studies.

For in vivo imaging, mice were lightly anesthetized with 2 L/min of 5% isoflurane in medical grade oxygen. Once mice were no longer ambulatory, they were transferred to a Perkin-Elmer IVIS Spectrum In Vivo Imaging System (Caliper Life Sciences, Perkin-Elmer) and kept under anesthesia at 1 L/min of 5% isoflurane in medical grade oxygen. Mice were imaged dorsally. Three mice were killed 8 d after injection to study biodistribution in secondary lymph organs, spleen, and iLN. The fluorescent radiant efficiency was quantified using the Living Image software (PerkinElmer).

In Vitro Uptake Assay. To make fluorescent NP peptide, 10 μL of 10 mg/mL Alexa Fluor 488 succinimidyl ester dye (Thermo Fisher) in DMSO was added to 50 μL of 2.1 mg/mL NP peptide in sterile DPBS. The reaction was stirred at 800 rpm for 1 h at room temperature on a Thermo-shaker (Grant Instruments), and excess dye was removed by buffer exchanging against over 100 volumes DPBS in a 3-kD diafiltration tube (Merck Millipore) until the filtrate was colorless.

Protein concentration was measured by BCA assay kit (Prod No. 23235; Thermo Scientific), and the conjugated dye concentration was measured by fluorescence against a standard curve of the free dye on a spectrophotometer (BioTek). To make fluorescent nanoparticles, 144-μg fluorescent NP peptide was added to 336-μg NP peptide (30% fluorescent NP peptide by mass) and used to create nanoparticles as described above.

JAWS-II dendritic cells were incubated with 100 μg/mL fluorescent NP-peptide nanoparticle, fluorescent soluble NP peptide, or DPBS as a negative control for 6 h. Cells were then washed with DPBS three times, fixed by 80% acetone in DPBS for 15 min, and washed twice more. DAPI at 1 μg/mL was used to stain the cells and incubated for 30 min at room temperature. After washing three times with DPBS, the cells were imaged using a fluorescent microscope BZ-X710 (Keyence).

Statistical Analysis. All data plotted with error bars are expressed as means with SD. The *P* values were generated by analyzing data with a two-tail unpaired *t* test, or two-way ANOVA using the Prism 5 program (GraphPad software). The survival rate statistical analysis was performed with a log-rank test.

Data Availability. The authors declare that the data supporting the findings of this study are available within the article and its *SI Appendix* file.

ACKNOWLEDGMENTS. We thank Robert Simmons and Ping Jiang from the Institute of Biomedical Science, Georgia State University, for excellent technical assistance and conceptual advice; and Gilbert Xavier Gonzalez from Institute of Biomedical Science, Georgia State University for his help in writing and editing this manuscript. This work was supported by the Institute of Biomedical Science, Georgia State University and by Grants R01AI101047 and R01AI116835 (to B.-Z.W.) from the National Institutes of Health.

1. Pan Y, et al. (2017) Influenza vaccination in preventing outbreaks in schools: A long-term ecological overview. *Vaccine* 35:7133–7138.
2. Teitzel G (2018) The moving target of flu. *Cell* 172:1139–1141.
3. Zhang H, Wang L, Compans RW, Wang BZ (2014) Universal influenza vaccines, a dream to be realized soon. *Viruses* 6:1974–1991.
4. Zheng M, Luo J, Chen Z (2014) Development of universal influenza vaccines based on influenza virus M and NP genes. *Infection* 42:251–262.
5. Sridhar S, et al. (2013) Cellular immune correlates of protection against symptomatic pandemic influenza. *Nat Med* 19:1305–1312.
6. Altenburg AF, Rimmelzwaan GF, de Vries RD (2015) Virus-specific T cells as correlate of (cross-)protective immunity against influenza. *Vaccine* 33:500–506.
7. Forrest BD, et al. (2008) Correlation of cellular immune responses with protection against culture-confirmed influenza virus in young children. *Clin Vaccine Immunol* 15: 1042–1053.
8. Antrobus RD, et al. (2014) Coadministration of seasonal influenza vaccine and MVA-NP+M1 simultaneously achieves potent humoral and cell-mediated responses. *Mol Ther* 22:233–238.
9. Deng L, Cho KJ, Fiers W, Saelens X (2015) M2e-based universal influenza A vaccines. *Vaccines (Basel)* 3:105–136.
10. Wang BZ, et al. (2014) Microneedle delivery of an M2e-TLR5 ligand fusion protein to skin confers broadly cross-protective influenza immunity. *J Control Release* 178:1–7.
11. Wang BZ, et al. (2012) Enhanced influenza virus-like particle vaccines containing the extracellular domain of matrix protein 2 and a Toll-like receptor ligand. *Clin Vaccine Immunol* 19:1119–1125.
12. Wang L, et al. (2013) Virus-like particles containing the tetrameric ectodomain of influenza matrix protein 2 and flagellin induce heterosubtypic protection in mice. *BioMed Res Int* 2013:686549.
13. Zhong W, Reed C, Blair PJ, Katz JM, Hancock K; Influenza Serology Working Group (2014) Serum antibody response to matrix protein 2 following natural infection with 2009 pandemic influenza A(H1N1) virus in humans. *J Infect Dis* 209:986–994.
14. De Filette M, et al. (2006) Improved design and intranasal delivery of an M2e-based human influenza A vaccine. *Vaccine* 24:6597–6601.
15. Sahdev P, Ochyl LJ, Moon JJ (2014) Biomaterials for nanoparticle vaccine delivery systems. *Pharm Res* 31:2563–2582.
16. Wang L, et al. (2017) Coated protein nanoclusters from influenza H7N9 HA are highly immunogenic and induce robust protective immunity. *Nanomedicine (Lond)* 13: 253–262.
17. Wang L, et al. (2014) Nanoclusters self-assembled from conformation-stabilized influenza M2e as broadly cross-protective influenza vaccines. *Nanomedicine (Lond)* 10: 473–482.
18. Wilson JT, et al. (2013) pH-responsive nanoparticle vaccines for dual-delivery of antigens and immunostimulatory oligonucleotides. *ACS Nano* 7:3912–3925.
19. Thomas SN, et al. (2011) Engineering complement activation on polypropylene sulfide vaccine nanoparticles. *Biomaterials* 32:2194–2203.
20. Uto T, et al. (2011) The induction of innate and adaptive immunity by biodegradable poly(γ-glutamic acid) nanoparticles via a TLR4 and MyD88 signaling pathway. *Biomaterials* 32:5206–5212.
21. Desai KG, Schwendeman SP (2013) Active self-healing encapsulation of vaccine antigens in PLGA microspheres. *J Control Release* 165:62–74.

22. Francis JN, et al. (2015) A novel peptide-based pan-influenza A vaccine: A double blind, randomised clinical trial of immunogenicity and safety. *Vaccine* 33:396–402.
23. Marshall S, Sahm LJ, Moore AC (2016) The success of microneedle-mediated vaccine delivery into skin. *Hum Vaccin Immunother* 12:2975–2983.
24. Prausnitz MR (2017) Engineering microneedle patches for vaccination and drug delivery to skin. *Annu Rev Chem Biomol Eng* 8:177–200.
25. Leone M, Mönkäre J, Bouwstra JA, Kersten G (2017) Dissolving microneedle patches for dermal vaccination. *Pharm Res* 34:2223–2240.
26. Norman JJ, et al. (2014) Microneedle patches: Usability and acceptability for self-vaccination against influenza. *Vaccine* 32:1856–1862.
27. Deng L, et al. (2018) Double-layered protein nanoparticles induce broad protection against divergent influenza A viruses. *Nat Commun* 9:359.
28. Schotsaert M, et al. (2016) Long-lasting cross-protection against influenza A by neuraminidase and M2e-based immunization strategies. *Sci Rep* 6:24402.
29. Schotsaert M, et al. (2013) Natural and long-lasting cellular immune responses against influenza in the M2e-immune host. *Mucosal Immunol* 6:276–287.
30. Deliyannis G, et al. (2006) Intranasal lipopeptide primes lung-resident memory CD8+ T cells for long-term pulmonary protection against influenza. *Eur J Immunol* 36: 770–778.
31. Jeon SH, Ben-Yedidia T, Arnon R (2002) Intranasal immunization with synthetic recombinant vaccine containing multiple epitopes of influenza virus. *Vaccine* 20: 2772–2780.
32. Wei H, Lenz SD, Thompson DH, Pogranichniy RM (2014) DNA-epitope vaccine provided efficient protection to mice against lethal dose of influenza A virus H1N1. *Viral Immunol* 27:14–19.
33. Van den Hoecke S, et al. (2017) Hierarchical and redundant roles of activating FcγRs in protection against influenza disease by M2e-specific IgG1 and IgG2a antibodies. *J Virol* 91:e02500-16.
34. van der Maaden K, et al. (2018) Hollow microneedle-mediated micro-injections of a liposomal HPV E743-63 synthetic long peptide vaccine for efficient induction of cytotoxic and T-helper responses. *J Control Release* 269:347–354.
35. Herrera-Rodriguez J, et al. (2018) A novel peptide-based vaccine candidate with protective efficacy against influenza A in a mouse model. *Virology* 515:21–28.
36. DiLillo DJ, Palese P, Wilson PC, Ravetch JV (2016) Broadly neutralizing anti-influenza antibodies require Fc receptor engagement for in vivo protection. *J Clin Invest* 126: 605–610.
37. Kallewaard NL, et al. (2016) Structure and function analysis of an antibody recognizing all influenza A subtypes. *Cell* 166:596–608.
38. Zhu W, et al. (2017) A boosting skin vaccination with dissolving microneedle patch encapsulating M2e vaccine broadens the protective efficacy of conventional influenza vaccines. *J Control Release* 261:1–9.
39. Pearton M, et al. (2010) Influenza virus-like particles coated onto microneedles can elicit stimulatory effects on Langerhans cells in human skin. *Vaccine* 28:6104–6113.
40. Chang TZ, Stadmiller SS, Staskevicius E, Champion JA (2017) Effects of ovalbumin protein nanoparticle vaccine size and coating on dendritic cell processing. *Biomater Sci* 5:223–233.
41. Estrada LH, Chu S, Champion JA (2014) Protein nanoparticles for intracellular delivery of therapeutic enzymes. *J Pharm Sci* 103:1863–1871.
42. Langer K, et al. (2008) Human serum albumin (HSA) nanoparticles: Reproducibility of preparation process and kinetics of enzymatic degradation. *Int J Pharm* 347:109–117.
43. Langer K, et al. (2003) Optimization of the preparation process for human serum albumin (HSA) nanoparticles. *Int J Pharm* 257:169–180.
44. Storp Bv, Engel A, Boeker A, Ploeger M, Langer K (2012) Albumin nanoparticles with predictable size by desolvation procedure. *J Microencapsul* 29:138–146.
45. Tsoras AN, Champion JA (2018) Cross-linked peptide nanoclusters for delivery of oncofetal antigen as a cancer vaccine. *Bioconjug Chem* 29:776–785.
46. Pandey AP, et al. (2017) Optimization of desolvation process for fabrication of lactoferrin nanoparticles using quality by design approach. *Artif Cells Nanomed Biotechnol* 45:1–14.
47. Coughlan L, et al. (2018) Heterologous two-dose vaccination with simian adenovirus and poxvirus vectors elicits long-lasting cellular immunity to influenza virus A in healthy adults. *EBioMedicine* 29:146–154.
48. Smith LR, et al. (2010) Phase 1 clinical trials of the safety and immunogenicity of adjuvanted plasmid DNA vaccines encoding influenza A virus H5 hemagglutinin. *Vaccine* 28:2565–2572.
49. Offit PA, Hackett CJ (2003) Addressing parents' concerns: Do vaccines cause allergic or autoimmune diseases? *Pediatrics* 111:653–659.
50. Qi M, et al. (2018) Intranasal nanovaccine confers homo- and hetero-subtypic influenza protection. *Small* 14:e1703207.
51. Varypataki EM, et al. (2016) Synthetic long peptide-based vaccine formulations for induction of cell mediated immunity: A comparative study of cationic liposomes and PLGA nanoparticles. *J Control Release* 226:98–106.
52. De Filette M, et al. (2008) An influenza A vaccine based on tetrameric ectodomain of matrix protein 2. *J Biol Chem* 283:11382–11387.
53. Fan Y, Moon JJ (2015) Nanoparticle drug delivery systems designed to improve cancer vaccines and immunotherapy. *Vaccines (Basel)* 3:662–685.
54. Irvine DJ, Swartz MA, Szeto GL (2013) Engineering synthetic vaccines using cues from natural immunity. *Nat Mater* 12:978–990.
55. Demento SL, et al. (2012) Role of sustained antigen release from nanoparticle vaccines in shaping the T cell memory phenotype. *Biomaterials* 33:4957–4964.
56. Littauer EQ, et al. (2018) Stable incorporation of GM-CSF into dissolvable microneedle patch improves skin vaccination against influenza. *J Control Release* 276:1–16.
57. Sullivan SP, et al. (2010) Dissolving polymer microneedle patches for influenza vaccination. *Nat Med* 16:915–920.
58. Rouphael NG, et al.; TIV-MNP 2015 Study Group (2017) The safety, immunogenicity, and acceptability of inactivated influenza vaccine delivered by microneedle patch (TIV-MNP 2015): A randomised, partly blinded, placebo-controlled, phase 1 trial. *Lancet* 390:649–658.
59. Vassilieva EV, et al. (2015) Improved immunogenicity of individual influenza vaccine components delivered with a novel dissolving microneedle patch stable at room temperature. *Drug Deliv Transl Res* 5:360–371.
60. Wacker M, et al. (2011) A toolbox for the upscaling of ethanolic human serum albumin (HSA) desolvation. *Int J Pharm* 414:225–232.
61. Geh KJ, Hubert M, Winter G (2016) Optimisation of one-step desolvation and scale-up of gelatine nanoparticle production. *J Microencapsul* 33:595–604.
62. Deng L, et al. (2017) Protein nanoparticle vaccine based on flagellin carrier fused to influenza conserved epitopes confers full protection against influenza A virus challenge. *Virology* 509:82–89.
63. Committee for the Update of the Guide for the Care and Use of Laboratory Animals IfLAR; Division of Earth and Life Sciences; National Research Council of the National Academies (2011) *Guide for the Care and Use of Laboratory Animals* (The National Academies Press, Washington, DC), 8th Ed.
64. Grcević D, Lee SK, Marusić A, Lorenzo JA (2000) Depletion of CD4 and CD8 T lymphocytes in mice in vivo enhances 1,25-dihydroxyvitamin D3-stimulated osteoclast-like cell formation in vitro by a mechanism that is dependent on prostaglandin synthesis. *J Immunol* 165:4231–4238.
65. Reed LJ, Muench H (1938) A simple method of estimating fifty per cent endpoints. *Am J Epidemiol* 27:493–497.